Accelerated fast BOTDA assisted by compressed sensing and image denoising

Hua Zheng, Yaxi Yan, Zhiyong Zhao, Tao Zhu, Jingdong Zhang, Nan Guo, Chao Lu

***Abstract*—We propose and experimentally demonstrate a scheme for accelerated fast BOTDA. The effect of signal-to-noise ratio (SNR) on recovery performance of compressed sensing is simulated and analyzed, it is found that a reduction in SNR requires much larger frequency data to recover the original Brillouin gain spectrum (BGS). To enable a high recovery probability, Block-Matching and 3D filtering (BM3D) algorithm is employed to enhance the SNR of Brillouin time trace and reduce the number of averages. Combining with a principal component analysis (PCA) based compressed sensing technique, the Brillouin gain spectrum (BGS) can be successfully reconstructed from only 37.5% frequency data. In the experiment, 75 randomly selected frequency data is acquired to reconstruct the BGS. Distributed strain sensing is achieved over 15 km single-mode fiber with 3 m spatial resolution and 0.52 MHz Brillouin frequency shift (BFS) uncertainty. Due to the accelerated process, the measurement time with 40 averages is less than 0.5 s.**

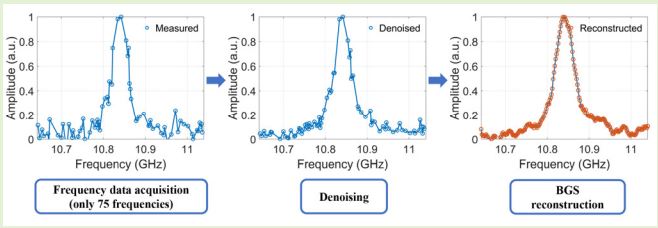

***Index Terms*—Brillouin optical time-domain analysis (BOTDA), compressed sensing, ultra-fast measurement**

I. Introduction

Brillouin scattering based distributed optical fiber sensors (DOFS) have attracted intensive research interests in the past several decades due to their potential applications in structural health monitoring (SHM) of large structures such as gas/oil pipelines, dams, and bridges [1]–[3]. As one of the typical Brillouin scattering based DOFS, Brillouin optical time-domain analysis (BOTDA) has the advantages of high signal-to-noise ratio (SNR) and long measuring range [4]–[6]. However, the acquisition process of BOTDA is quite time-consuming since it requires the mapping of Brillouin gain spectrum (BGS) step-by-step over a wide frequency range. To solve this problem, numerous dynamic sensing techniques have been presented. Among them, slope-assisted BOTDA [7]–[10], sweep free BOTDA [11]–[13], and optical chirp chain BOTDA [14]–[16] omit the frequency sweeping process and thus can substantially boost the sensing speed. Image denoising methods which utilizes redundancies and correlations contained in the two-dimensional (2D) data have also been proposed in recent years. Several conventional algorithms as well as deep-learning based algorithms have been successfully implemented for DOFS signal denoising such as nonlocal mean [17], wavelet denoising (WD) [18], Block-Matching and 3D filtering (BM3D) [19], and CNN [20]. Alternatively, fast BOTDA still involves frequency sweeping to reconstruct the BGS while employing a frequency-agile technique to reduce the frequency switching time [21]–[25]. Acquisition rates from several hundred to several thousand hertz have been demonstrated. However, the sensing range is limited to a few hundred meters. For long-range sensing, the number of scanning frequencies and trace averaging limit the further improvement of the sampling rate.

More recently, compressed sensing (CS) based BOTDA is proposed. Since the BGS, which has a Lorentzian lineshape, is sparse in the discrete cosine transform (DCT) domain, it can be recovered from few measurement data through an orthogonal matching-pursuit (OMP) algorithm. It was demonstrated that only 30% of the frequency data was required to reconstruct the entire BGS, which greatly reduced the acquisition time as well as the amount of data to store [26]. Principal component analysis (PCA) based CS has also been proposed to improve the performance of fast BOTDA since BGS shows better sparsity level in PCA sparse base. BGS with 4 MHz frequency step and 500 MHz span was successfully recovered from 30% randomly sampled frequency data [27]. Besides, a signal is always affected by the noise in practical measurements, which deteriorates the recovery performance of CS, especially in the low SNR scenario (i.e., long-range BOTDA).

In this paper, we propose and experimentally demonstrate a scheme of accelerated fast BOTDA assisted by CS and image denoising. The effect of SNR on the recovery performance of CS is analyzed. It is found that a reduction in SNR requires much larger frequency data to recover the BGS. Therefore, Block-matching and 3D filtering (BM3D) is employed to

This work was supported by General Research Fund PolyU 152168/17E of the Hong Kong SAR government; project ZVGB of the Hong Kong Polytechnic University; National Natural Science Foundation of China (61905030); China Postdoctoral Science Foundation (2019M663435); Natural Science Foundation Project of Chongqing (cstc2019jcyj–bshX0001).

H. Zheng, Y. Yan, Z. Zhao and C. Lu are with the Department of Electronic and Information Engineering, The Hong Kong Polytechnic University, Kowloon, Hong Kong, China.

T. Zhu, J Zhang, N. Guo are with the Key Laboratory of Optoelectronic Technology & Systems (Ministry of Education), Chongqing University, Chongqing 400044, China.

enhance the SNR of the time trace. In the experiments, 37.5% randomly selected frequency data is acquired and pre-denoised by using BM3D to reconstruct the BGS along the sensing fiber. Distributed strain sensing is achieved over 15 km single-mode fiber with 3 m spatial resolution and the measurement time with 40 averages is less than 0.5 s.

II. Principle

CS is a sampling paradigm that allows to simultaneously measure and compress signals that are sparse or compressible in some domains. Consider a one-dimensional signal x, which can be viewed as an $N\times 1$ column vector with element $x[n]$, n=1, 2, …, N. x can be expressed as [28]–[30]:

$$x = \sum_{i=1}^{N} s_i \psi_i = \Psi s \tag{1}$$

Where $\Psi=\{\psi_1, \psi_2, \ldots, \psi_N\}$ is an $N\times N$ matrix constructed by a series of basis $\{\psi_i\}$, s is the coefficient sequence of x. The signal x is known as K sparse signal over the dictionary Ψ only if s is a vector with all except K of its elements as zero. The CS theory exploits that most signals of interest are sparse or compressible in the sense that they can be encoded with just a few coefficients without much numerical or perceptual loss. In order to reconstruct the signal x, a set of M measurements that are linear functionals of x is acquired. More precisely

$$y = \Phi x = \Phi\Psi s = As \tag{2}$$

Φ is a $M\times N$ matrix with $M<N$, which refer as the measurement matrix. The CS theory proves that when the matrix $A=\Phi\Psi$ has the Restricted Isometry Property (RIP), the s or the signal x can be recovered from measurements y with high probability. In practical measurement, a signal is inevitably corrupted by ambient and system noise. In light of that, Eq. (2) can be rewritten as [31]:

$$y = Ax + n = A(x + n_s) + n_m \tag{3}$$

In which $n=An_s+n_m$, while n_s and n_m denote the signal and the measurement noise, respectively. Assume that n_s and n_m are independent zero-mean Gaussian noise with variance σ_s^2 and σ_m^2, respectively. The covariance matrix $\mathbf{\Sigma}$ of the total noise vector n becomes

$$\mathbf{\Sigma} = \sigma_s^2 AA^T + \sigma_m^2 I_M \tag{4}$$

Where I_M represents an $M\times M$ identity matrix. In a special case, when the rows of A are orthogonal with an equal norm of $\sqrt{N/M}$, the noise n is white with covariance

$$\mathbf{\Sigma} = \frac{1}{\rho}\sigma_s^2 I_M + \sigma_m^2 I_M = (\frac{1}{\rho}\sigma_s^2 + \sigma_m^2) I_M \tag{5}$$

In which $\rho=M/N$. From (5), it can be seen that the variance of the signal noise after compression increases by the factor of N/M, which is known as the noise folding effect [32], [33]. Thus, the performance of the CS recovery algorithms depends seriously on the number of measurements and the input SNR. When the SNR of the input signal is low, the recovery probability will decrease rapidly.

For a BOTDA system, the ideal BGS has a Lorentzian lineshape which is shown in Fig. 1(a) (blue circle). The BGS is comprised of 200 frequency points, which corresponds to a total measurement range of 398 MHz with 2 MHz frequency step. The full width at half maximum (FWHM) of BGS is set to 40 MHz. It can be translated to a sparse signal s by using PCA transform. Fig. 1(b) shows the property of s, it can be observed that the amplitude of s converges to zero rapidly, only a few elements of s are not zero.

To test the performance of CS technique, OMP algorithm is employed to reconstruct the BGS. Fig. 2(a) shows the ideal BGS with N=200 data points, and the red circles in Fig. 2(a) are 75 randomly selected data points and the reconstructed result is shown in Fig. 2(b). The reconstructed BGS is in perfect agreement with the original BGS, which means that the BGS can be reliably reconstructed despite using a few data points.

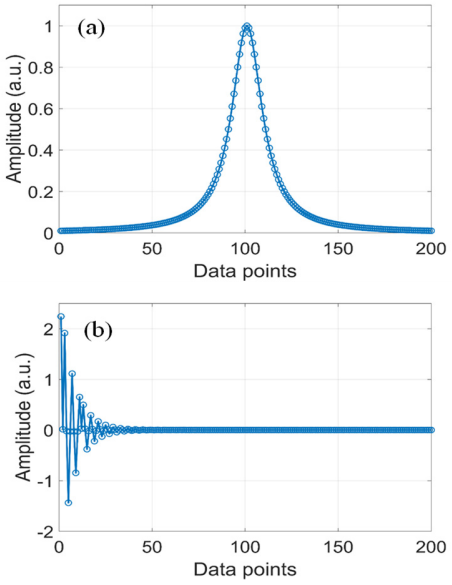

Fig. 1. (a) Original BGS with 200 data points and a linewidth of 40 MHz. (b) The sparse representation of BGS obtained through PCA transform.

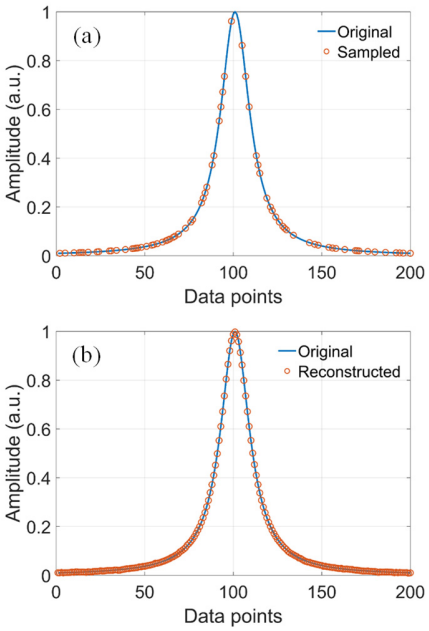

Fig. 2. (a) Original BGS (blue line) and the randomly selected data points (red dots). (b) Reconstructed BGS by using OMP algorithm (red dots).

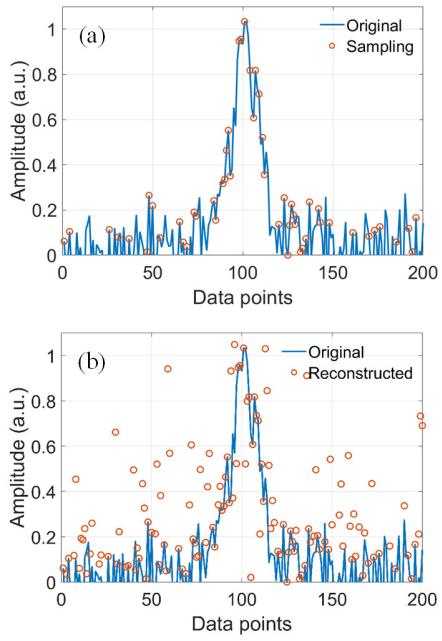

Fig. 3. (a) Noise-affected BGS with an SNR of 10 dB (blue line) and the randomly selected data points (red dots). (b) Reconstructed noisy BGS (red dots).

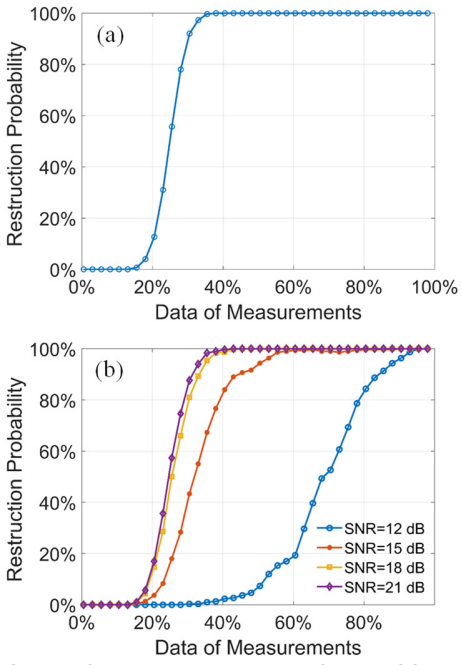

Fig. 4. (a) Successful recovery percentage of ideal BGS as a function of the measurement numbers. (b) The successful recovery percentage of BGS with different SNRs as a function of the measurement numbers.

However, in BOTDA measurement, the acquired frequency data is always noisy, especially for the long-range scenario. Fig. 3(a) shows a noisy BGS with an SNR of 10 dB, and Fig. 3(b) is the reconstructed result. It can be seen that when the SNR is relatively low, large errors will arise in the recovered BGS. The correlation coefficient between the original BGS and the reconstructed one is only 0.58.

To investigate the effect of SNR on CS, simulations are performed to analyze the successful recovery rate (100 trials spectra) of BGS as a function of the measurement numbers and the results are shown in Fig. 4. As expected, when the SNR decreases, a higher percentage of the measurement number is necessary to guarantee the spectrum recovery. For the BGS with SNR of 21 dB, 94% successful recovery rate can be achieved with the number of frequency acquisitions only 33% of that needed by a conventional BOTDA. On the other hand, for BGS with 12 dB SNR, the required number of random measurements increases to 88% of the full frequency acquisitions to recover the spectrum with high probability.

III. Experimental Setup

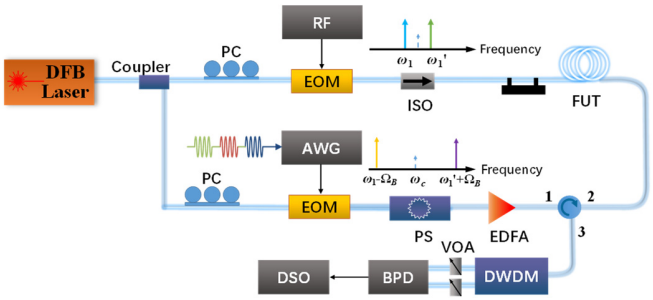

Fig. 5. Experimental setup. PC: polarization controller, EOM: electro-optic modulator, RF: radio frequency source, AWG: arbitrary waveform generator, PS: polarization scrambler, EDFA: Erbium-doped fiber amplifier, ISO: isolator, FUT: fiber under test, DWDM: dense wavelength division multiplexer, VOA: variable optical attenuator, DSO: digital storage oscilloscope.

The experimental setup is shown in Fig. 5. A narrow linewidth distributed feedback (DFB) laser operating at 1549.1 nm is used as the light source. The output of the laser is divided into two propagation paths by using a 3dB optical coupler. The upper branch signal is used as the probe and the lower branch signal is used as the pump. In the lower branch, microwave pulse trains generated by an AWG with 12 GSa/s sampling rate are modulated onto the pump light through a high extinction ratio (i.e., > 40 dB) electro-optic modulator (EOM) biased at the null-transmission point. In order to fast scan the Brillouin spectral response, the frequency of pump is modulated from 250 MHz to 648 MHz with a step of 2 MHz by using frequency-agile technique. The pulse width and repetition frequency are 30 ns and 9 kHz, respectively. Then the pump pulses are amplified by using an erbium-doped fiber amplifier (EDFA) before launching them into the fiber under test (FUT).

In the upper branch, the probe is modulated by a radio frequency signal with frequency fixed at 11.29 GHz. After propagating through the FUT, the upper and lower sidebands of the probe wave are separated by using a dense wavelength division multiplexer (DWDM) with a bandwidth of 100 GHz and then detected by a balanced photodetector (BPD) with 200-MHz bandwidth. Since both pump and probe waves are performed double-side-band (DSB) modulation, the upper sideband of probe will interact with the upper sideband of pump via loss process, while the lower sideband of probe will interact with the lower sideband of pump via gain process. After

balanced detection, the SNR can be improved and the larger undesirable DC component will also be removed [34]. The electrical signals output from the PD are collected by a digital storage oscilloscope (DSO) with 200 MHz sampling rate (limited by the storage depth of DSO) and the acquired data are sent to a computer for further processing.

15 km single-mode fiber whose BFS is around 10.84 GHz at room temperature is served as FUT. Near the end of the fiber, a section of 6 m is stretched by two translation stages.

IV. Experimental Results and Discussions

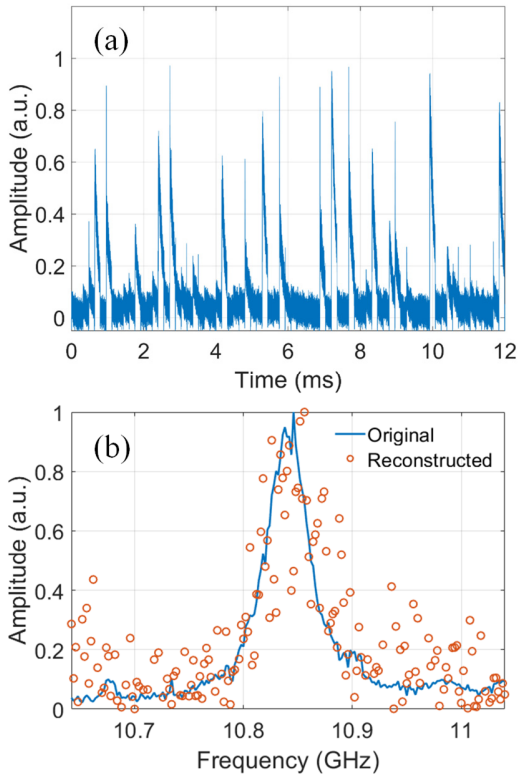

Fig. 6. (a) Acquired Brillouin signal of the 75 randomly selected frequencies (40 averages). (b) Measured (blue line, 2560 averages) and reconstructed BGS (red dots) at 15 km.

To verify the reconstruction performance of OMP algorithm, the Brillouin time-domain traces of the 75 randomly selected frequencies are acquired as shown in Fig.6 (a), the SNR at the end of fiber is estimated to about 11.6 dB (40 averages). Fig. 6 (b) shows the measured BGS by using the conventional frequency sweeping method (blue line, 2560 averages) and reconstructed BGS (red dots) from raw data in Fig. 6(a) at 15 km, respectively. As expected in theoretical analysis, the reconstructed BGS is seriously distorted due to the low SNR, the correlation coefficient between the measured BGS and reconstructed BGS is only 0.78. After Lorentzian curve fitting, the BFS difference of the two BGSs is 5.9 MHz (10.8409 GHz for measured BGS and 10.8468 GHz for reconstructed BGS), which means that the reconstructed BGS from low SNR signal will generate a large error.

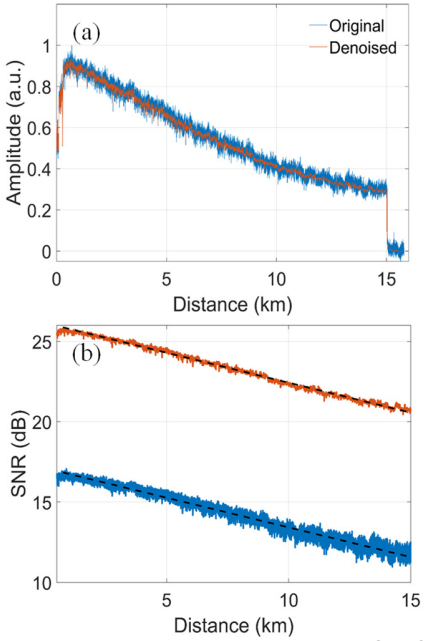

Fig. 7. (a) Acquired Brillouin time trace around BFS before (blue line) and after (red line) denoising by using BM3D. (b) The SNR of Brillouin time trace before (blue line) and after (red line) denoising. The black dashed lines show linear fitting (in dB scale) of the SNR curves versus distance.

Here, BM3D is used to further enhance the SNR of Brillouin trace [19]. BM3D includes three main operations: block matching, collaborative filtering and reconstruction. In block matching, BM3D utilizes non-local principle to group similar blocks together to reveal self-similarity of original blocks (or patches) in the image. Then the matching blocks of the image are stacked into a 3-Dimensional array, which will be processed by the following collaborative filtering in the transform domain. Collaborative filtering could remove the noise efficiently but still preserves most of the significant details in the original image. After collaborative filtering, noise-reduced blocks in the 3D array are mapped back to their original location with an appropriate weighting of the overlapping blocks. Since the 75 frequencies are discretely distributed, BM3D cannot be used directly in case of blurring the information between adjacent frequencies. The time serves as a second dimension and a two-dimensional (2D) image is formed by stacking 80 successive measurements of each frequency. The size of a block in BM3D is set to 8 × 8 pixels while the search window is restricted to the size of 39×39 pixels in order to reduce the computational complexity. In collaborative filtering process, 3D discrete cosine transform (DCT) is applied to obtain the coefficients of the 3D blocks. A hard threshold of 3.5 σ (i.e., the standard deviation of the noise) is used to remove the noise, Wiener filtering is used after the hard thresholding. The denoising result is shown in Fig.7 (a) (red line), it can be seen from the figure that the noise in the recovered signals is greatly suppressed. Fig. 7(b) compares the SNRs of the raw noisy traces (blue lines) and the ones obtained after denoising (red lines) with the BM3D. The black dashed lines correspond to the respective linear fitting (in dB scale) of the SNR versus distance curves. The

results indicate that an SNR at 15 km on the raw data can be substantially boosted to 22 dB. Although the denoising is performed in time dimension, the SNR in BGS domain can be equally improved [35].

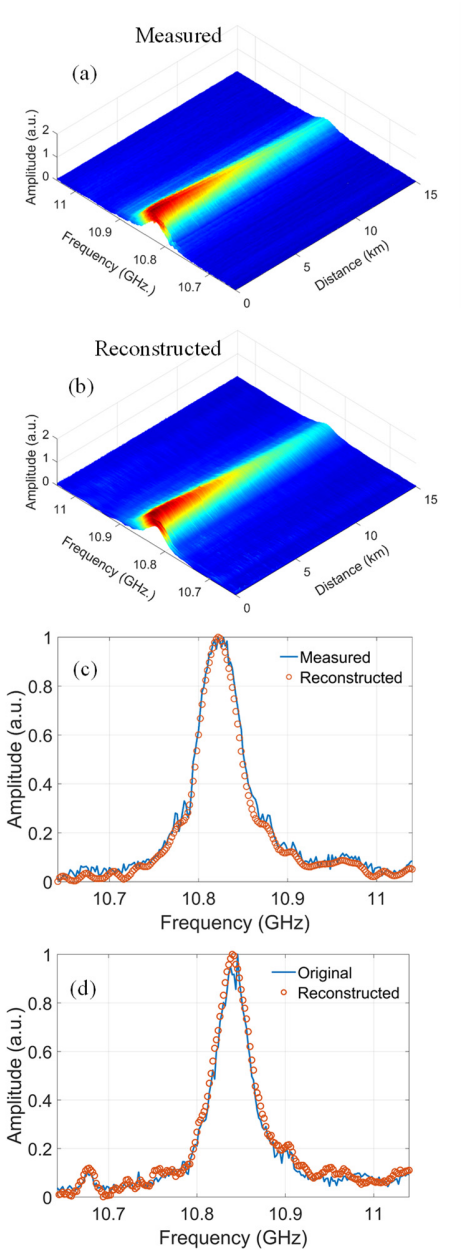

Fig. 8. (a) BGS distribution along FUT obtained by using frequency sweeping method with 2 MHz frequency step and 200 frequency acquisitions. Each time-trace is averaged 2560 times. (b) BGS distribution along FUT reconstructed by using 75 randomly selected frequencies. (c) Measured (blue line) and reconstructed (red line) BGS at 0.2 km. (d) Measured (blue line) and reconstructed (red line) BGS at 15 km.

Fig. 8(a) shows the measured BGS by entirely acquiring 200 frequencies (2560 averages), Fig. 8(b) depicts the reconstructed BGS distribution along FUT by using the denoised 75 frequencies in Fig. 7. The correlation coefficient between the two figures is 0.9909 which validates that the OMP algorithm can successfully reconstruct the BGS by using only 37.5% of the total frequency data. Fig. 8(c) and (d) show the BGSs at 0.2 km and 15 km, respectively. The reconstructed BGS agree well with the measured spectra and no relevant distortion is observed. Thus, the entire acquisition time can be greatly reduced to about 0.5 s.

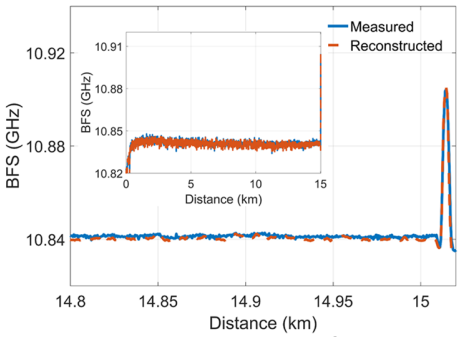

Fig. 9. The measured and reconstructed BFS distribution along the last 220 m fiber section (inset: the distribution of BFS along the FUT).

Fig. 9. shows the acquired BFS from the measured BGS (blue line) and the reconstructed BGS (red dash line). We can observe that the fitting results agree well with each other, thus verifying the reliability of the CS reconstruction. The stretched section can be clearly identified and the BFS difference between the stretched and unstretched fiber is found to be 64 MHz. The ~3 m transition section also implies a spatial resolution of 3 m. Fig. 9 inset gives the BFS distribution along the FUT. The BFS uncertainty (i.e., the standard deviation of the BFS values around the last 30 m fiber section) of measured and reconstructed results are calculated to be 0.5 MHz and 0.52 MHz, respectively.

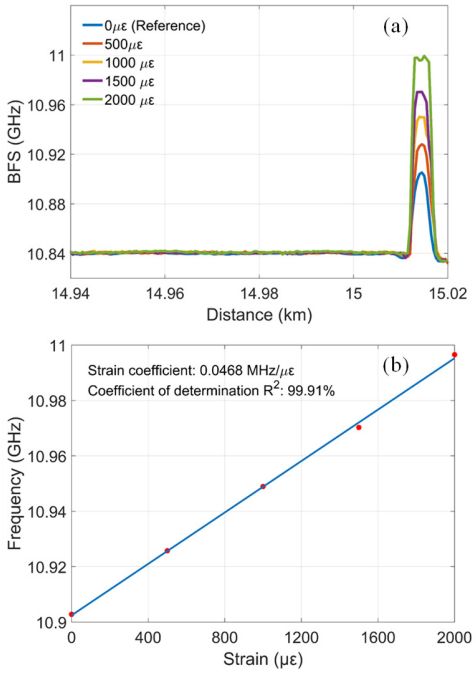

Fig. 10. (a) Estimated BFS along the stretched fiber with different strains (all reconstructed by using 75 selected frequency data). (b) BFS of the stretched fiber as a function of strain. Blue line is the linear curve fitting.

Distributed strain sensing experiments are also carried out to test the performance of F-BOTDA. Near the end of the FUT, a section of 6 m is stretched, where the strain is increased in steps of 500 με. The results are depicted in Fig. 10(a) which shows that when the strain grows larger, the BFS shifts upwards. Fig. 10(b) shows the linear fitting result of BFS as a function of strain via linear fitting. The strain coefficient for the FUT is 0.0468 MHz/με. The coefficient of determination R^2 is 99.91%, indicating that a good linear relationship is achieved for the strain sensing.

We also summarize the overall performance of fast BOTDA reported to data as shown in table I. Compared with previous works, the sensing range of fast BOTDA is significantly improved by exploiting BM3D and CS methods in this scheme.

TABLE I
KEY PARAMETERS OF FAST BOTDA REPORTED TO DATA

	Spatial resolution	Sensing range	BFS uncertainty	Dynamic range	Sensing speed
Ref.21	1.3 m	100 m	0.25 MHz	200 MHz	0.1 ms
Ref.22	0.2 m	50 m	0.7 MHz	200 MHz	0.07 ms
Ref. 23	1.5 m	145 m	0.5 MHz	210 MHz	0.6 ms
Ref.24	1.5 m	2 km	0.74 MHz	147 MHz	2.3 ms
This work	3 m	15 km	0.52 MHz	398 MHz	0.45 s

V. Conclusion

In this paper, we proposed and experimentally demonstrated a scheme of accelerated fast BOTDA. The effect of signal-to-noise ratio (SNR) on recovery performance of compressed sensing is verified both in simulation and experiment. It is found that a reduction in SNR requires much larger frequency data to recover the original Brillouin gain spectrum (BGS). To enable a high recovery probability, Block-Matching and 3D filtering (BM3D) algorithm is employed to enhance the SNR of Brillouin time trace. In this way, both the number of trace averaging and scanning frequencies are dramatically reduced. BGS over 15 km single-mode fiber can be measured with only 40 averages and 37.5% frequency data (75 points) within 0.5 s. The spatial resolution, BFS uncertainty, and dynamic range are 3 m, 0.52 MHz, and 398 MHz respectively. The proposed method can significantly enhance the performance of BOTDA without any hardware modifications.

References

[1] J. M. López-Higuera, L. R. Cobo, A. Q. Incera, and A. Cobo, "Fiber optic sensors in structural health monitoring," *J. Light. Technol.*, vol. 29, no. 4, pp. 587–608, 2011.

[2] H. N. Li, D. S. Li, and G. B. Song, "Recent applications of fiber optic sensors to health monitoring in civil engineering," *Eng. Struct.*, vol. 26, no. 11, pp. 1647–1657, 2004.

[3] A. Barrias, J. R. Casas, and S. Villalba, "A review of distributed optical fiber sensors for civil engineering applications," *Sensors*, vol. 16, no. 5, p. 748, 2016.

[4] M. A. Soto, G. Bolognini, F. Di Pasquale, and L. Thévenaz, "Simplex-coded BOTDA fiber sensor with 1 m spatial resolution over a 50 km range," *Opt. Lett.*, vol. 35, no. 2, pp. 259–261, 2010.

[5] Y. Dong, L. Chen, and X. Bao, "Time-division multiplexing-based BOTDA over 100km sensing length," *Opt. Lett.*, vol. 36, no. 2, pp. 277–279, 2011.

[6] M. A. Soto, G. Bolognini, and F. Di Pasquale, "Long-range simplex-coded BOTDA sensor over 120km distance employing optical preamplification," *Opt. Lett.*, vol. 36, no. 2, pp. 232–234, 2011.

[7] R. Bernini, A. Minardo, and L. Zeni, "Dynamic strain measurement in optical fibers by stimulated Brillouin scattering," *Opt. Lett.*, vol. 34, no. 17, pp. 2613–2615, 2009.

[8] D. Zhou *et al.*, "Slope-assisted BOTDA based on vector SBS and frequency-agile technique for wide-strain-range dynamic measurements," *Opt. Express*, vol. 25, no. 3, pp. 1889–1902, 2017.

[9] D. Ba *et al.*, "Distributed measurement of dynamic strain based on multi-slope assisted fast BOTDA," *Opt. Express*, vol. 24, no. 9, pp. 9781–9793, 2016.

[10] H. Zheng *et al.*, "Distributed vibration measurement based on a coherent multi-slope-assisted BOTDA with a large dynamic range," *Opt. Lett.*, vol. 44, no. 5, pp. 1245–1248, 2019.

[11] A. Voskoboinik, O. F. Yilmaz, A. W. Willner, and M. Tur, "Sweep-free distributed Brillouin time-domain analyzer (SF-BOTDA)," *Opt. Express*, vol. 19, no. 26, pp. B842–B847, 2011.

[12] C. Jin *et al.*, "Scanning-free BOTDA based on ultra-fine digital optical frequency comb," *Opt. Express*, vol. 23, no. 4, pp. 5277–5284, 2015.

[13] J. Fang, P. Xu, Y. Dong, and W. Shieh, "Single-shot distributed Brillouin optical time domain analyzer," *Opt. Express*, vol. 25, no. 13, pp. 15188–15198, 2017.

[14] D. Zhou *et al.*, "Single-shot BOTDA based on an optical chirp chain probe wave for distributed ultrafast measurement," *Light Sci. Appl.*, vol. 7, no. 1, pp. 1–11, 2018.

[15] Y. Dong *et al.*, "150 km fast BOTDA based on the optical chirp chain probe wave and Brillouin loss scheme," *Opt. Lett.*, vol. 43, no. 19, pp. 4679–4682, 2018.

[16] B. Wang *et al.*, "High-performance optical chirp chain BOTDA by using a pattern recognition algorithm and the differential pulse-width pair technique," *Photonics Res.*, vol. 7, no. 6, pp. 652–658, 2019.

[17] M. A. Soto, J. A. Ramirez, and L. Thévenaz, "Intensifying the response of distributed optical fibre sensors using 2D and 3D image restoration," *Nat. Commun.*, vol. 7, no. 1, pp. 1–11, 2016.

[18] X. Qian *et al.*, "Long-range BOTDA denoising with multi-threshold 2D discrete wavelet," in *Asia-Pacific Optical Sensors Conference*, 2016, pp. W4A-24.

[19] H. Wu, L. Wang, Z. Zhao, N. Guo, C. Shu, and C. Lu, "Brillouin optical time domain analyzer sensors assisted by advanced image denoising techniques," *Opt. Express*, vol. 26, no. 5, pp. 5126–5139, 2018.

[20] H. Wu *et al.*, "Real-time denoising of Brillouin optical time domain analyzer with high data fidelity using convolutional neural networks," *J. Light. Technol.*, vol. 37, no. 11, pp. 2648–2653, 2019.

[21] Y. Peled, A. Motil, and M. Tur, "Fast Brillouin optical time domain analysis for dynamic sensing," *Opt. Express*, vol. 20, no. 8, pp. 8584–8591, 2012.

[22] Y. Dong *et al.*, "High-spatial-resolution fast BOTDA for dynamic strain measurement based on differential double-pulse and second-order sideband of modulation," *IEEE Photonics J.*, vol. 5, no. 3, pp. 2600407–2600407, 2013.

[23] I. Sovran, A. Motil, and M. Tur, "Frequency-scanning BOTDA with ultimately fast acquisition speed," *IEEE Photonics Technol. Lett.*, vol. 27, no. 13, pp. 1426–1429, 2015.

[24] H. Zheng *et al.*, "Fast distributed Brillouin optical fiber sensing based on pump frequency modulation," *Appl. Phys. Express*, vol. 11, no. 7, p. 072502, 2018.

[25] H. Zheng *et al.*, "Polarization independent fast BOTDA based on pump frequency modulation and cyclic coding," *Opt. Express*, vol. 26, no. 14, pp. 18270–18278, 2018.

[26] D. P. Zhou, W. Peng, L. Chen, and X. Bao, "Brillouin optical time-domain analysis via compressed sensing," *Opt. Lett.*, vol. 43, no. 22, pp. 5496–5499, 2018.

[27] Q. Chu, B. Wang, H. Wang, D. Ba, and Y. Dong, "Fast Brillouin optical time-domain analysis using frequency-agile and compressed sensing," *Opt. Lett.*, vol. 45, no. 15, pp. 4365–4368, 2020.

[28] R. G. Baraniuk, “Compressive sensing [lecture notes],” *IEEE Signal Process. Mag.*, vol. 24, no. 4, pp. 118–121, 2007.
[29] S. Ji, Y. Xue, and L. Carin, “Bayesian compressive sensing,” *IEEE Trans. Signal Process.*, vol. 56, no. 6, pp. 2346–2356, 2008.
[30] T. Jihua, S. Jinping, Z. Yuxi, N. Ahmad, and S. Xiaoyang, “The effects of input signal-to-noise ratio on compressive sensing SAR imaging,” in *2010 2nd International Conference on Signal Processing Systems*, 2010, vol. 3, pp. V3-533.
[31] A. Lavrenko, F. Römer, G. Del Galdo, and R. Thomä, “On the SNR variability in noisy compressed sensing,” *IEEE Signal Process. Lett.*, vol. 24, no. 8, pp. 1148–1152, 2017.
[32] E. A. Castro and Y. C. Eldar, “Noise folding in compressed sensing,” *IEEE Signal Process. Lett.*, vol. 18, no. 8, pp. 478–481, 2011.
[33] M. A. Davenport, J. N. Laska, J. R. Treichler, and R. G. Baraniuk, “The pros and cons of compressive sensing for wideband signal acquisition: Noise folding versus dynamic range,” *IEEE Trans. Signal Process.*, vol. 60, no. 9, pp. 4628–4642, 2012.
[34] A. Domínguez-López, A. López-Gil, S. Martín-López, and M. González-Herráez, “Signal-to-noise ratio improvement in BOTDA using balanced detection,” *IEEE Photonics Technol. Lett.*, vol. 26, no. 4, pp. 338–341, 2013.
[35] M. A. Farahani, M. T. Wylie, E. Castillo-Guerra, and B. G. Colpitts, “Reduction in the number of averages required in BOTDA sensors using wavelet denoising techniques,” *J. Light. Technol.*, vol. 30, no. 8, pp. 1134–1142, 2011.